The influence of V defects on luminescence properties of AlInGaN quaternary alloys

2005 J. Phys.: Condens. Matter 17 729

(http://iopscience.iop.org/0953-8984/17/4/015)

INSTITUTE OF PHYSICS PUBLISHING JOURNAL OF PHYSICS: CONDENSED MATTER

J. Phys.: Condens. Matter **17** (2005) 729–736 doi:10.1088/0953-8984/17/4/015

The influence of V defects on luminescence properties of AlInGaN quaternary alloys

C B Soh[1], S J Chua[1,2,3], S Tripathy[2], W Liu[2] and D Z Chi[2]

[1] Centre for Optoelectronics, Department of Electrical and Computer Engineering, National University of Singapore, 117576, Singapore
[2] Institute of Materials Research and Engineering, 3 Research Link, 117602, Singapore

E-mail: elecsj@nus.edu.sg

Received 18 October 2004
Published 14 January 2005
Online at stacks.iop.org/JPhysCM/17/729

Abstract

In a certain growth mode, V pits have been observed in $Al_yIn_xGa_{1-x-y}N$ grown by metal–organic chemical vapour deposition. Room temperature photoluminescence (PL) spectra from these quaternary alloys show strong band-to-band emission with equally intense yellow luminescence (YL). Simultaneous measurements of the PL intensity and topography using ultraviolet–visible near field scanning optical microscopy show that the enhanced YL intensity originates from the V pits whereas the intensity of the band edge PL decreases in the vicinity of pits. The strong YL emission can be related to the defect clusters associated with impurity decoration at dislocation lines and sidewalls of the pits. A higher degree of Al incorporation at partially filled V pits leads to the multiple near band edge PL peaks.

(Some figures in this article are in colour only in the electronic version)

1. Introduction

III–V nitride based materials have attracted a lot of research interest relating to their use in blue–green and ultraviolet light emitting diodes (LEDs) and laser diodes (LDs). Recent development of AlGaN/GaN heterostructures and quaternary $In_xAl_yGa_{1-x-y}N$ layers has led to the successful fabrication of ultraviolet light emitting devices in the wavelength range 280–360 nm. These short wavelength light emitting devices can be used in areas such as optical data storage, lithography, biomedical instrumentation and sensors. The use of ternary $Al_xGa_{1-x}N$ layers at high molar fractions of Al is limited by the larger band offset and the high polarization charges (pyroelectric and piezoelectric) at the interface [1, 2]. Furthermore, lattice mismatch-induced tensile stress was observed during the growth of AlGaN heterostructures on GaN, leading to relaxation through crack generation [3]. Various groups have reported the growth

[3] Author to whom any correspondence should be addressed.

of AlInGaN layers on sapphire substrates [4–7]. The use of the quaternary alloy allows for independent control of the lattice mismatch in $In_xAl_yGa_{1-x-y}N$/InGaN/GaN based structures while keeping built-in strain below the critical value.

Fluctuations in the composition profiles and growth parameters can give rise to surface pits commonly known as V defects. These V defects have been observed in InGaN as well as InGaN/GaN quantum well structures [8–11]. The vertex of the V defect has been found to originate from threading dislocations. These threading dislocations disrupt the InGaN MQW and affect its luminescence efficiency [12, 13]. On the basis of first-principles calculations, Northrup proposed that the V defect formation is enhanced by the segregation of In on the $(10\bar{1}1)$ facets [14]. Recently, Pécz *et al* observed V-shaped surface pits on AlGaN different from those on InGaN due to presence of segregated Al atoms within the pits [15]. Besides the influence of such defects on surface morphology, the spatial distribution of the quantum well blue emission and yellow luminescence are strongly related to the distribution of V defects in the epilayer [16]. Further study is needed to determine whether the threading dislocations linked to the vertex of the V defect serve as an effective non-radiative recombination centre or enhance the compositional fluctuation [17, 18].

Photoluminescence (PL) and cathodoluminescence (CL) techniques are commonly employed to investigate the optical properties of these nitrides. Conventional far field PL imaging techniques are affected by a diffraction phenomenon, which limits the lateral resolution to approximately 0.5 μm. However, using near field scanning optical microscopy (NSOM), it is possible to achieve spatial resolution of the order of 50–100 nm. The NSOM has the capability of mapping the topography simultaneously with the PL intensity and hence can provide a correlation of the spatial distribution of PL images with the topographic features. Recently, Liu *et al* have investigated V pits in AlInGaN quaternary alloys using CL spectroscopy [19]. In this study, we report the optical characterization of AlInGaN/GaN heterostructures grown on sapphire substrates using NSOM and PL measurements.

2. Experiment

The $Al_yIn_xGa_{1-x-y}N$ quaternary alloy films ($x = 0.01$, $y = 0.05$–0.07) were grown by metal–organic chemical vapour deposition (MOCVD). A LT GaN buffer layer was first grown to a thickness of 35 nm at 550 °C and then a 2 μm thick undoped GaN layer was deposited at 1050 °C. This was followed by the growth of 150 nm thick quaternary layers at 850 °C. The NSOM system is implemented for ultraviolet–visible imaging and spectrally resolved emission has been detected by using a photomultiplier tube. The details of the set-up are described elsewhere [20]. The surface morphology of the layers was also studied with a Digital Instruments Nanoscope III AFM set-up operating in the tapping mode. Micro-PL spectra of $Al_yIn_xGa_{1-x-y}N$ quaternary films were recorded using a Renishaw 2000 micro-PL set-up equipped with the 325 nm line of a He–Cd laser.

In order to determine the composition of the $Al_yIn_xGa_{1-x-y}N$ quaternary alloy, the ternary alloys $Al_{0.05}Ga_{0.95}N$ and $In_{0.01}Ga_{0.99}N$ were grown. The flow rates of trimethylgallium (TMGa) and trimethylaluminium (TMAl) were kept constant for the growth of $Al_{0.05}Ga_{0.95}N$ and $Al_{0.05}In_{0.01}Ga_{0.94}N$, as it is assumed that the flow of these precursors will be the dominant factor influencing the growth rate. A similar approach was used for $In_{0.01}Ga_{0.99}N$. The films were characterized using PL and x-ray diffraction (XRD) to determine the band gap and the lattice constant of the quaternary alloy. Using Vegard's law and the relationship established by Aumer *et al* [21], the film composition was determined. The thickness of the AlInGaN layer was also obtained from SIMS depth profiling.

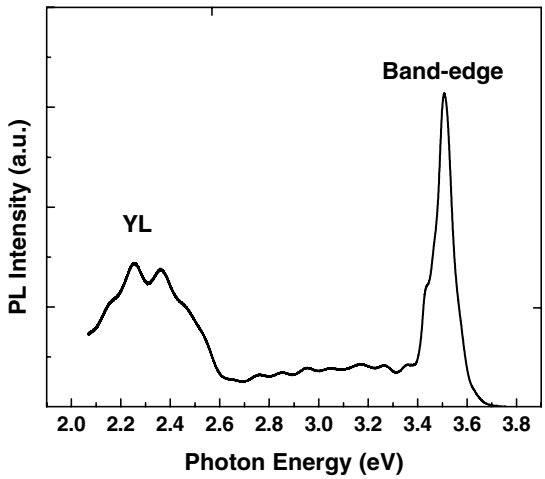

Figure 1. Room temperature micro-PL spectra of $Al_{0.05}In_{0.01}Ga_{0.94}N$ showing strong band edge emission near 354 nm (3.508 eV) and YL centred around 545 nm (2.27 eV).

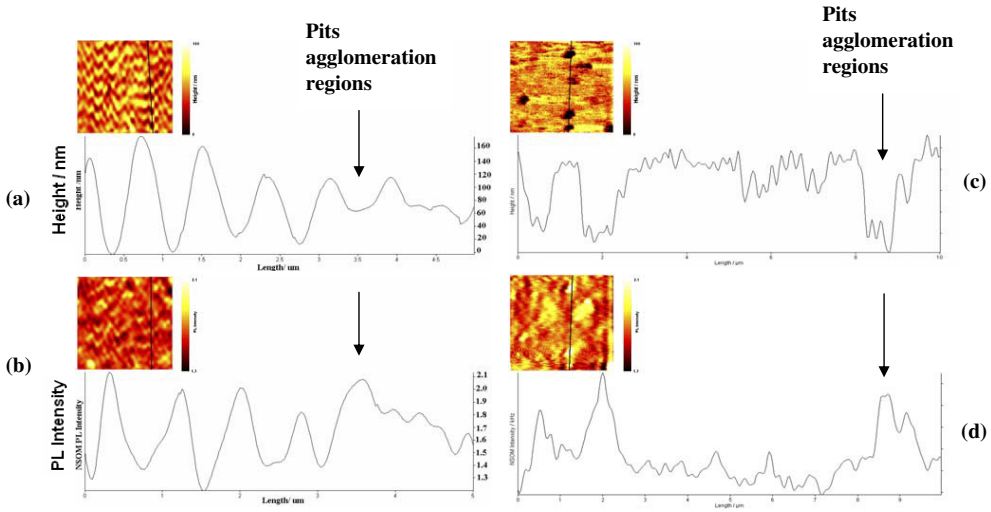

Figure 2. (a) NSOM topography of $Al_{0.05}In_{0.01}Ga_{0.94}N$ with a probe aperture of 100 nm showing agglomeration of the surface pits; (b) a NSOM PL intensity image at 550 nm of $Al_{0.05}In_{0.01}Ga_{0.94}N$ showing the spatial variation of the YL intensity; (c) NSOM topography of $Al_{0.07}In_{0.01}Ga_{0.92}N$ with a probe aperture of 100 nm; and (d) a NSOM PL intensity image at 550 nm of $Al_{0.07}In_{0.01}Ga_{0.92}N$. Cross-section line scans of the topography and PL intensity image selected from the micrographs are marked with straight lines.

3. Results and discussion

Figure 1 shows the micro-PL spectra of the $Al_{0.05}In_{0.01}Ga_{0.94}N$ quaternary film at room temperature. The sharp band edge emission peak is observed near 354 nm (3.508 eV). The spectra also show a broad yellow luminescence (YL) centred around 545 nm (2.27 eV). In order to address the microscopic optical properties associated with the V pit distribution in our quaternary samples, ultraviolet–visible NSOM measurements were carried out at room temperature as shown in figure 2. The topographic images in figure 2 show surface pits of

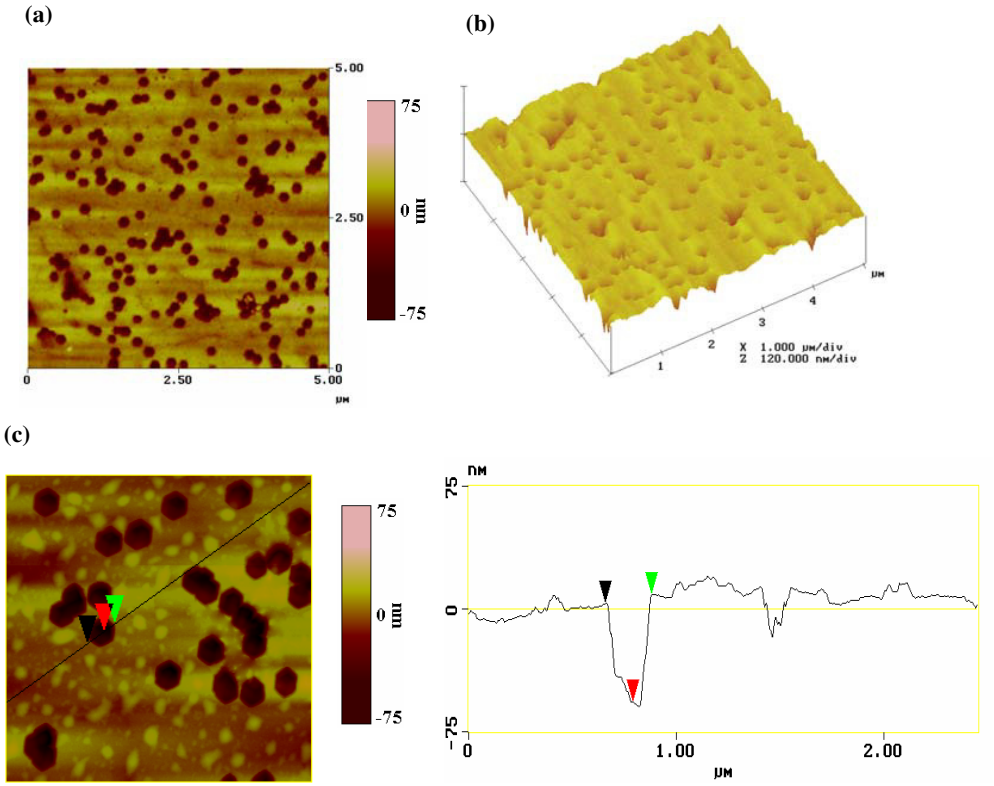

Figure 3. (a) 5.0 μm $\times$ 5.0 μm 2D and (b) 3D AFM images of $Al_{0.05}In_{0.01}Ga_{0.94}N$ recorded using a Digital Nanoscope 3000 system. The micrograph in (a) shows 270 pits. (c) The pit depth is estimated from the cross-sectional profile of a 2.0 μm $\times$ 2.0 μm AFM line scan.

diameter $\sim$0.2 μm. The NSOM PL image recorded at 550 nm (band pass filter 540–560 nm) shows that YL emission is enhanced inside the pits and pit agglomeration can be seen from the cross-section topographic and luminescence images. In the NSOM PL image, the YL peak intensity varies on an arbitrary scale from 1.3 to 2.1 and shows strong spatial variation.

The lateral resolution in the topographic NSOM image taken using the fibre optic probe (tip aperture $\sim$50–100 nm) is inferior to that for the silicon tip ($\sim$5 nm) commonly used in a conventional high resolution AFM set-up. To address this difference, the lateral structures obtained from the NSOM set-up were compared with AFM measurements obtained using a Digital Instruments Nanoscope 3000. The results from the NSOM agree with the topography analysis shown in figure 3, where surface pits and their agglomeration are also observed over the scanned region. The rms roughness for the surface is estimated to be $\sim$15 nm, giving an average pit depth of $\sim$70 nm and a diameter of $\sim$0.25 μm. The dislocation density has been estimated to be 1.0×10^9 cm^{-2} on the basis of the pit count ($\sim$270 pits) over the region of 5×5 μm^2 shown in figure 3(a). This agrees quite well with the dislocation density of about 6.8×10^8 cm^{-2} estimated from the x-ray diffraction spectra using Ayers' model [22], where the FWHM values for the x-ray rocking curves for the symmetrical and asymmetrical planes were analysed. From these results, it is confirmed that surface pits are in some way related to the dislocations threading from the GaN template during the growth of the quaternary alloy. In figure 4, dark field cross-section TEM imaging along $\mathbf{g} = 0002$ and the zone axis

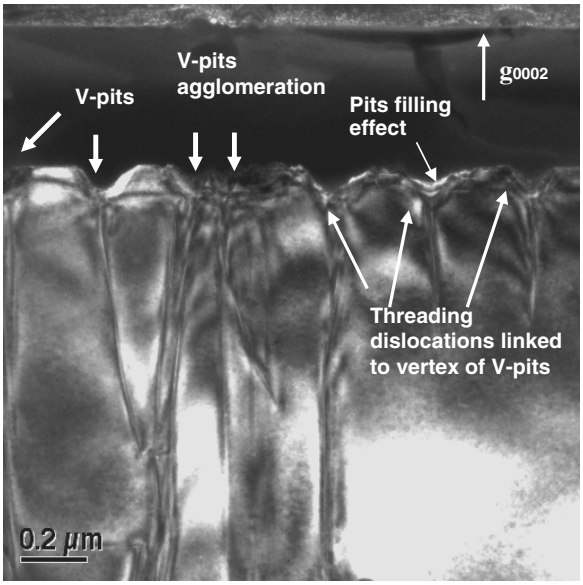

Figure 4. A dark field transmission electron microscopy (TEM) image under reflection $g = (0002)$ at the zone axis $[2\bar{1}\bar{1}0]$. The image shows the existence of V pits with dislocations linked to its vertex.

$[2\bar{1}\bar{1}0]$ shows threading dislocations which are mainly of mixed and screw type linked to the vertices of the V pits. It was also observed that some of the dislocations are terminated before reaching the epilayer. Gliding of threading dislocations along different planar directions leads to dislocation branching and the formation of more surface pits. V pit formation serves as a mechanism for relaxation of these terminated dislocations. In figure 3(b), cross-sectional atomic force microscopy images over a 2.0 μm $\times$ 2.0 μm region show that these pits are not completely conical but are truncated in shape. Such filling of pits is found to be associated with segregation of Al around dislocations. The determination of the elemental composition at the truncated V pits by energy dispersive x-ray spectroscopy (EDX) has indicated a higher Al incorporation in $Al_yIn_xGa_{1-x-y}N$, which is approximately a 20%–30% increment from that of the pit free region. However, due to the relatively low In and Al incorporation, the variation in the elemental composition is not prominent. Hence truncated V pits in our quaternary sample are different from the commonly observed inverted hexagonal pits found in InGaN epilayers [8–13].

In the NSOM instrument, the emission over a wavelength range of 335–450 nm, which covers the emission from the band edge of the quaternary alloy, is also mapped with the topography. Figure 5 shows the correlation of the near field topography (figure 5(a)) and the PL intensity images (figure 5(b)) over the band edge region. The band edge PL intensity varies on an arbitrary scale from 0.1 to 1.1. There is a decrease in the band edge luminescence intensity from the pits. The band edge emission is slightly brighter at the perimeter of the pits and away from the pits the band edge emission is relatively uniform over the scanned region. This shows that there is no compositional fluctuation over the region without surface pits and there is an absence of inhomogeneity caused by substitution of In. Using the 514.5 nm excitation, a micro-Raman spectrum for the sample was also recorded using a JY T64000 set-up. The spectrum does not indicate the presence of InGaN-like A_1 (LO) and AlGaN-like A_1 (LO) phonons as the compositions of Al and In are relatively low, which also confirms the

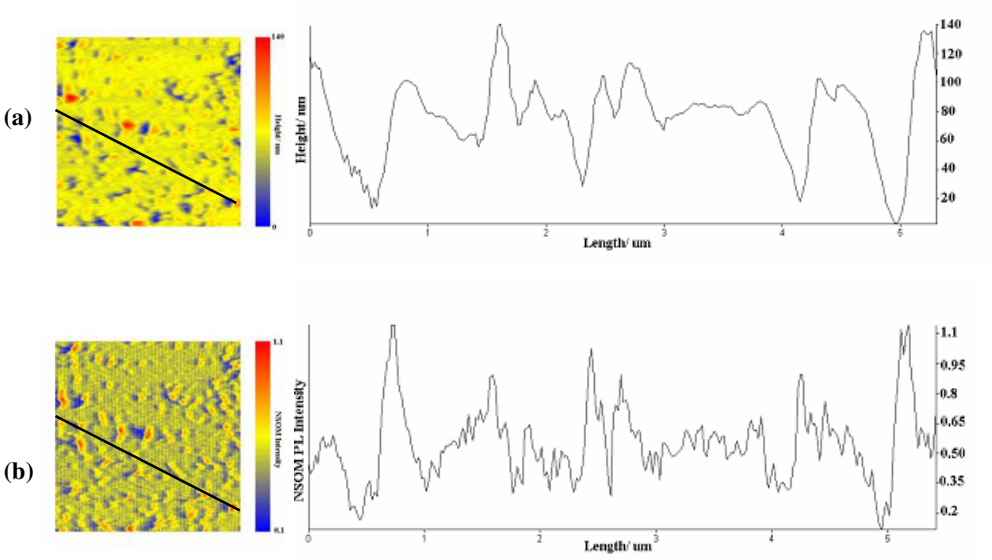

Figure 5. (a) NSOM topography of $Al_{0.05}In_{0.01}Ga_{0.94}N$ with a probe aperture of 50 nm, showing clearly the surface pits; (b) a NSOM PL intensity image showing the spatially varying band edge emission intensity. An optical filter in the wavelength range 335–450 nm was used along with a Raman edge filter to block the reflected light. By selecting the same region in these micrographs, marked with straight lines, it is seen that the cross-sections of the PL intensity image correlate well with the topography.

absence of In clusters. Therefore, in the regions without surface pits, a relatively uniform band edge PL intensity has been detected by NSOM.

To further investigate the luminescence properties, PL measurements for the $In_xAl_yGa_{1-x-y}N$ quaternary alloy were carried out in the temperature range 10–300 K. The temperature dependent PL spectra are shown in figure 6. At 13 K, a dominant PL peak, labelled as 'P_1', attributed to the quaternary alloy was detected at 3.574 eV together with a lower emission peak at ∼3.489 eV due to the underlying GaN epilayer. An additional peak, 'P_2', detected at 3.607 eV can be related to emission from regions of higher Al content, which is likely to be at the V pit sites. The nonuniformity in the composition, especially that of the Al content, could also explain the AlInGaN emission peaks near 3.535 eV ('P_3'), 3.574 eV ('P_1') and 3.607 eV ('P_2'). The PL spectrum also displays additional GaN-like LO phonon replicas. This phenomenon is attributed to the confinement by and subsequent interaction of electron–hole pairs with the AlGaN-like lattice. To address the possible optical transition mechanisms, temperature dependent PL analysis of the sample has also been carried out, as shown in figure 6(b). The PL peak energy decreases with increase in the temperature. Varshni's relation [23] can be fitted well to all the peaks. This implies an absence of localized states [24] in our quaternary sample and the fitting using Varshni's equation, $E_g(T) = E_g(0) - \frac{\alpha T^2}{\beta + T}$, gives typical values of the fitting parameters $\beta \sim 997$ K and $\alpha \sim 7.9 \times 10^{-4}$ eV K^{-1} for the dominant AlInGaN band edge peak 'P_1'. From PL analyses, we have also seen a greater ease of non-radiative recombination of carriers from the existing trap levels, which accounts for the more drastic decrease in PL intensity with increase of the temperature. Impurity decoration along the dislocation lines and the sidewalls of V pits could have accounted for the strong YL band emission observed from the pits and could also be responsible for the subsequent decrease in the band edge emission. Such behaviour is related to the tendency of undergoing non-radiative

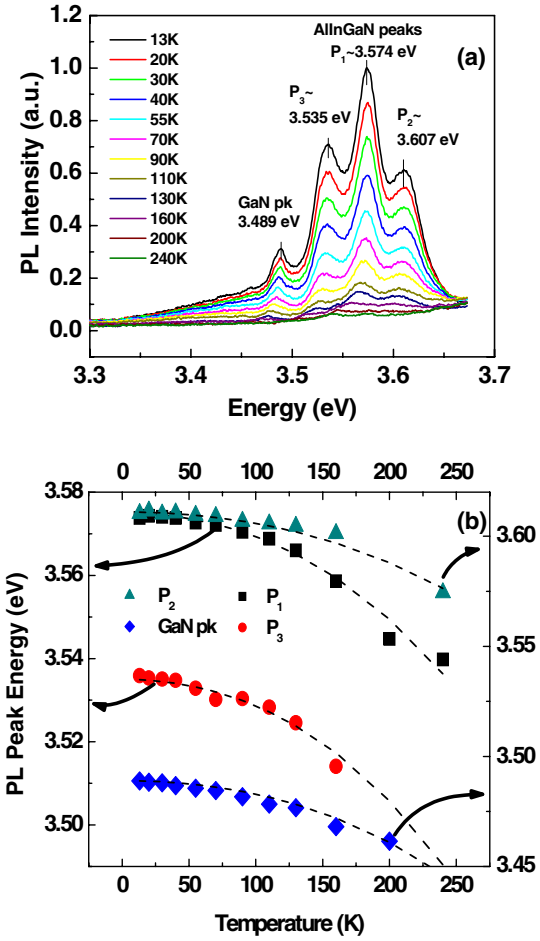

Figure 6. (a) Temperature dependent PL spectra of an $Al_{0.05}In_{0.01}Ga_{0.94}N$ sample. (b) Theoretical curve fitting following Varshni's equation for the variation of the band edge PL peaks as a function of temperature.

recombination especially at room temperature. Due to the fact that the dislocations are likely to be charged, there is also a possibility that these impurities will interact with dislocations, leading to the formation of defect clusters along the dislocation lines and on the sidewalls of pits. This agrees with the proposed effect of dislocations on the intensities of both band edge luminescence and YL proposed by Shi *et al* [18]. We therefore believe that the YL is enhanced by the presence of V pits in our quaternary alloys. This competes with band edge PL emission (I_{BE}) from the quaternary alloy at the pits and their agglomeration sites and contributes to the reduction of the intensity ratio of the band edge and YL transitions. Due to the presence of impurities at the V pit sites, the YL shows strong spatial variation as observed in NSOM measurements.

4. Conclusions

In summary, the spatially resolved luminescence properties of the $Al_{0.05}In_{0.01}Ga_{0.94}N$ quaternary layer have been investigated. The enhanced yellow luminescence at the truncated

pits and at their agglomeration sites originates from impurity decoration especially at the threading dislocation lines. These impurities form energy states near the band edges and partly account for the spatial fluctuation in the near field band edge emission intensity. Anomalous multiple AlInGaN band edge emission peaks observed from 3.54 to 3.61 eV are due to the higher Al composition at the pits as compared to the other regions. This compositional fluctuation in the quaternary epilayer is partly related to strain relaxation at the pits, which leads to subsequent filling of V pits.

References

[1] Bernardini F, Fiorentini V and Vanderbilt D 1997 *Phys. Rev.* B **56** 10024
[2] Deguchi T, Sekiguchi K, Nakamura A, Sota T, Matsuo R, Chichibu S and Nakamura S 1999 *Japan. J. Appl. Phys.* **38** L914
[3] Han J, Crawford M H, Shul R J, Hearne S J, Chason E, Figiel J J and Banas M 1999 *Mater. Res. Soc. Internet J. Nitride Semicond. Res.* **4S1** G7.7
[4] McIntosh F G, Boutros K S, Roberts J C, Bedair S M, Piner E L and El-Masry N A 1996 *Appl. Phys. Lett.* **68** 40
[5] Asif Khan M, Yang J W, Simin G, Gaska R, Shur M S, Loye H C G, Tamulaitis G, Zukauskas A, Smith D J, Chandrasekhar D and Tassius R B 2000 *Appl. Phys. Lett.* **76** 1161
[6] Hirayama H, Kinoshita A, Yamabi T, Enomoto Y, Hirata A, Araki T, Nanishi Y and Aoyagi Y 2002 *Appl. Phys. Lett.* **80** 207
[7] Cremades A, Navarro V, Piqueras J, Lima A P, Ambacher O and Stutzmann M 2001 *J. Appl. Phys.* **90** 4868
[8] Watanabe K, Yang J R, Huang S Y, Inoke K, Hsu J T, Tu R C, Yamazaki T and Nakanishi N 2003 *Appl. Phys. Lett.* **82** 718
[9] Wu X H, Elsass C R, Abare A, Mack M, Keller S, Petroff P M, DenBaars S P, Speck J S and Rosner S J 1998 *Appl. Phys. Lett.* **72** 692
[10] Chen Y, Takeuchi T, Amano H, Akasaki I, Yamada N, Kaneko Y and Wang S Y 1998 *Appl. Phys. Lett.* **72** 710
[11] Kawaguchi Y, Shimizu M, Yamaguchi M, Hiramatsu K, Sawaski N, Taki W, Tsuda H, Kuwano N, Oki K, Zheleva T and Davis R F 1998 *J. Cryst. Growth* **189/190** 24
[12] Scholz F, Off J, Fehrenbacher E, Gfrőrer O and Brockt G 2000 *Phys. Status Solidi* a **180** 315
[13] Sharma N, Thomas P, Tricker D and Humphreys C 2000 *Appl. Phys. Lett.* **77** 1274
[14] Northrup J E, Romano L T and Neugebauer J 1999 *Appl. Phys. Lett.* **74** 2319
[15] Pecz B, Makkai Z, Forte-Poisson M A, Huet F and Dunin-Borkowski R E 2001 *Appl. Phys. Lett.* **78** 1529
[16] Jeong M S, Kim Y W, White J O, Suh E K, Cheong M G, Kim C S, Hong C H and Lee H J 2001 *Appl. Phys. Lett.* **79** 3440
[17] Narukawa Y, Kawakami Y, Funato M, Fujita S and Nakamura S 1997 *Appl. Phys. Lett.* **70** 981
[18] Shi JY, Yu L P, Wang Y Z, Zhang G Y and Zhang H 2002 *Appl. Phys. Lett.* **80** 293
[19] Liu J P, Wang Y T, Yang H, Jiang D S, Jahn U and Ploog K H 2004 *Appl. Phys. Lett.* **84** 5449
[20] Chua S J, Tripathy S, Chen P, Takasuka E and Ueno M 2004 *Physica* E **25** 356
[21] Aumer M E, LeBoeuf S F, McIntosh F G and Bedair S M 1999 *Appl. Phys. Lett.* **75** 3315
[22] Ayers J E 1994 *J. Cryst. Growth* **135** 71
[23] Varshni Y P 1967 *Physica* **34** 149
[24] Yaguchi H, Kikuchi S, Hijikata Y, Yoshida S, Aoki D and Onabe K 2001 *Phys. Status Solidi* b **228** 273